Uncertainty of the Pu to ^{244}Cm Ratio in Spent Fuel

Seung Min Woo and Joonhong Ahn

Department of Nuclear Engineering, University of California, Berkeley, Berkeley, California, 94720
sngminwoo@gmail.com

*The Pu-to-^{244}Cm ratio method is considered a non-destructive and indirect method for measurement of Pu mass for pyrometallurgical processing of spent nuclear fuel. The method utilizes the formula, Pu mass = (Pu/^{244}Cm) * (^{244}Cm mass), in which the ratio is to be estimated by numerical simulation of fuel depletion, while ^{244}Cm mass can be measured by counting its spontaneous fission neutrons. The uncertainty associated with the Pu-to-^{244}Cm ratio due to the non-uniform nuclide compositions in spent fuel rods and assemblies can significantly affect material accountancy. In this study, we have observed the non-uniform nuclide composition by numerical simulation with the numerical recipe that has been established with the depletion simulation code Serpent. Using this recipe, compositions in two fuel assemblies in the OPR-1000 reactor core under "extreme" conditions with respect to the burnup and initial enrichment are calculated to observe and understand physical processes of depletion. In the simulation result, significant variation is observed in mass densities of Pu and ^{244}Cm along the axial direction, particularly in the top and bottom of the fuel assembly. Based on the simulation result, change of uncertainty associated with the Pu-to-^{244}Cm ratio in the three pre-processing stages of the pyroprocessing, i.e., chopping, voloxidation, and homogenization, has been replicated by assuming mixing conditions in these stages. The standard deviations of Pu and ^{244}Cm mass densities and its ratios significantly decrease in the voloxidation process and are strongly dependent on mixing conditions.*

I. BACKGOUND AND OBJECTIVE

Nuclear material accountancy is a fundamental basis for safeguards against weapons proliferation (Ref. 1). Reliable material accountancy must be established before starting operation of a nuclear facility such as the pyrometallurgical processing system (Ref. 2). Among various methods suggested for Pu mass measurement in the pyroprocessing system, the Pu-to-^{244}Cm ratio method has been proposed (Ref. 3) based on the formula,

$$\left(\text{Pu mass}\right) = \left(\frac{\text{Pu}}{^{244}\text{Cm}}\right) \times \left(^{244}\text{Cm mass}\right). \qquad (1)$$

The mass of ^{244}Cm can be measured by the neutron-counting rate in spent fuel, because most of these neutrons are generated by the spontaneous fission of ^{244}Cm (Ref. 3). The Pu-to-^{244}Cm ratio is determined by burnup code calculation.

In this method, various causes of uncertainties can be considered. First, there are other neutron sources in spent fuel such as ^{240}Pu and ^{246}Cm (Ref. 3), so that the mass of ^{244}Cm would be overestimated. We must take into account errors with a neutron detector itself. These will cause uncertainties in ^{244}Cm (and consequently ^{239}Pu) mass measurement. The value of the ratio can vary significantly because of non-uniformity in spent fuel and batches at various stages of pyroprocessing (Ref. 4). Because the ratio is evaluated by numerical simulation, it is imperative to establish numerical models to accurately estimate non-uniformity of the ratio within a spent fuel assembly as well as the evaluation of the ratio through pyroprocessing stages. This will consist of detailed simulations for burnup of nuclear fuel and for the mass-flow simulations in the pyroprocessing system. For the former, in addition to non-uniformity in nuclide compositions resulting from conditions in the reactor core, uncertainty of input data such as cross-section data and design parameters associated with manufacturing uncertainties (Ref. 5) may also cause error. The computer simulation code used for the simulation may have numerical errors. In this study, we primarily focus on evaluating non-uniform nuclide compositions in spent fuel.

For non-uniformity in spent fuel, various relevant studies have been performed. The non-uniformity of burnup and power in assemblies of the Optimized Power Reactor (OPR)-1000 reactor core is discussed in Ref. 6. Nuclide compositions are compared between PWR and BWR and between UO_2 and MOX in Ref. 7. The burnup distribution in the axial direction for several different assemblies has been compared (Ref. 8). The axial non-uniformity of total fission rate (Ref. 9) and the radial power, burnup and compositions (Ref. 10) for the fuel pin are evaluated. The non-uniformity of power, burnup and nuclide compositions in spent fuel based on different scales, such as the core-, assembly-, and fuel pin-scale, has been studied. However, the impact of non-uniformity of nuclide composition in spent fuel on material accountancy has not been studied in detail. The purposes of this study are following;

- Observation of non-uniformity of nuclide composition in spent fuel.
- Analysis for understanding how the observed non-uniformity affects on material accountancy in the pyroprocessing.
- Assessment of safeguardability for the pyroprocess.

In this paper, the first and the beginning part of the second are mainly discussed.

II. METHODOLOGY AND MODELING FOR DEPLETION SIMULATION

The continuous-energy Monte Carlo depletion code, Serpent (Ref. 11), has been utilized to evaluate nuclide compositions in spent fuel. We have developed the numerical recipes for the depletion simulation (Ref. 12), which was benchmarked by comparing with the result of the previous studies (Refs. 13 and 14). In summary, the developed numerical recipes indicate that the single mesh in the radial direction and 1cm mesh size in the axial direction for the bottom and top of the fuel pin cell give sufficient accuracy and fidelity.

The depletion simulation should be conducted at an assembly scale, because, according to the conceptual design for the pyroprocess developed by Korea Atomic Energy Research Institute (KAERI), one PWR spent fuel assembly is handled in one campaign (Ref. 15). Among the 23 nuclear power plants in South Korea, 19 are PWRs. Of these, 11 are OPR-1000 (Ref. 16), including HANBIT units 3, 4, 5 and 6, and HANUL units 3, 4, 5, and 6. Therefore, we consider the OPR-1000 fuel assemblies, for which design parameters are shown in Table 1 (Ref. 6).

Table 1. Design parameters for OPR-1000 (Ref. 6).

Thermal power [MW]	2815
Specific power [kW/kgU]	36.91
Inlet temperature [^{o}C]	296.1
Avg. temperature [^{o}C]	312.2
Pellet material	UO_2
Pellet density [g/cm^3]	10.44
Pellet diameter [cm]	0.826
Clad inner diameter [cm]	0.843
Clad outer diameter [cm]	0.970
Cladding	ZIRLO
Active length [cm]	381
Fuel pitch [cm]	1.285
Fuel assembly	16X16

In the OPR-1000 reactor core, 14 different types of assemblies are loaded. The number of assemblies loaded into the core as a function of burnup at discharge and the initial enrichment is plotted in Fig. 1. The arrows indicate the case with the lowest burnup and the lowest initial fuel enrichment (A0 type assembly, brown color arrow), and the case with the 2nd highest burnup and the highest initial enrichment assembly (D0 type assembly, orange color arrow), respectively. Two assemblies are selected as the extreme cases to observe the ranges of nuclide compositions in spent fuel. The burnup and initial enrichment for two assemblies are shown in Table 2.

Table 2. Burnup and initial enrichment for two extreme assemblies

A004 assembly	Burnup [MWd/kgU]	Enrichment [%]	No. of rods
1st cycle	11.59	1.42	236
D009 assembly	Burnup [MWd/kgU]	Enrichment [%]	No. of rods
1st cycle	16.90	4.42/3.93	184/52
2nd cycle	34.61		
3rd cycle	51.24		

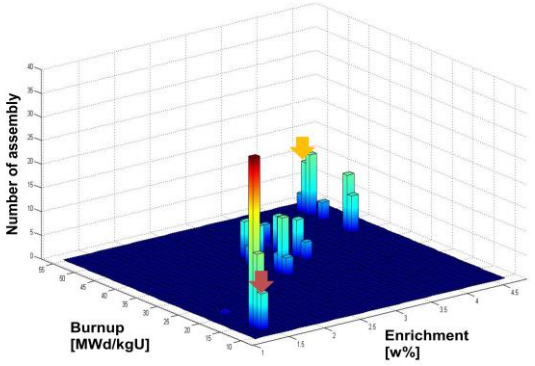

Fig. 1. Number of assemblies (z-axis) as a function of burnup (x-axis) and initial enrichment (y-axis).

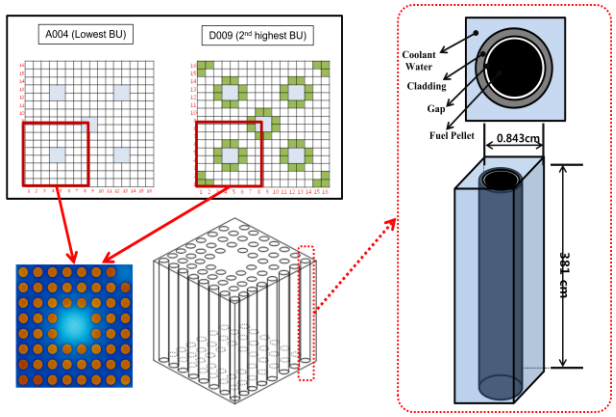

Fig. 2. Modeling of the quarter of assemblies for depletion simulation.

We have considered a quarter of an assembly, which consists of 59 fuel pin-cells, due to symmetry as shown in Fig. 2. Because no sufficient information is given in open literature, the additional assumptions are applied as follows;

- the cooling time between cycles is 60 days, and

- the assembly power output is constant during the cycles.

III. SIMULATION RESULTS FOR NUCLIDE COMPOSITION IN SPENT FUEL ASSEMBLIES

The Pu mass density of each fuel pin as a function of the normalized axial height is plotted for the A0 type assembly (low burnup case (LBU)) and the D0 type assembly (high burnup case (HBU)) in Fig. 3. The maximum and minimum Pu mass densities are 1.17E-1 and 4.70E-2 [g/cm^3] for the HBU, respectively. The maximum value is around 2.5 times greater than the minimum value. The maximum value is observed in the middle of the fuel rod, because the neutron flux is greater at the middle of the fuel rod than top and bottom. The averaged Pu mass density for the assembly is 1.08E-1 [g/cm^3], which is close to the value at the middle of the fuel rods. The Pu mass density for the LBU is generally less than the HBU due to the lower burnup. The maximum and minimum Pu mass densities for the LBU are 5.69E-2 and 1.38E-2 [g/cm^3], respectively. The maximum value is around 4 times greater than the minimum value. The difference between the maximum and minimum is greater in the case of LBU than HBU. Thus, the non-uniformity of Pu mass density in the axial direction of the fuel rod becomes more significant when the burn up is lower. The Pu mass density for the middle of the fuel rods is shown with flat plateaus, because of the large size mesh is applied for the depletion simulation. In reality, such a uniform distribution for the nuclide compositions in spent fuel rods is impossible. Therefore, in future studies, the large middle mesh should be discretized into the smaller meshes in order to estimate the nuclide compositions more practically.

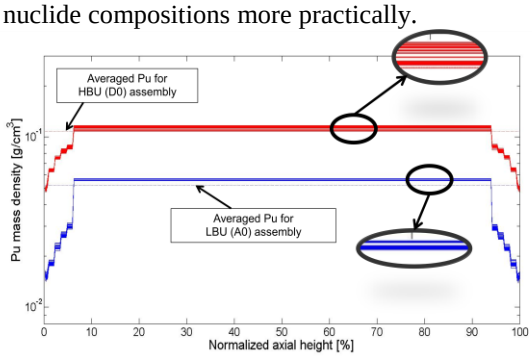

Fig. 3. Pu mass densities as a function of the normalized axial height for the D0 (HBU: High Burnup, red) and the A0 (LBU: Low Burnup, blue) assemblies

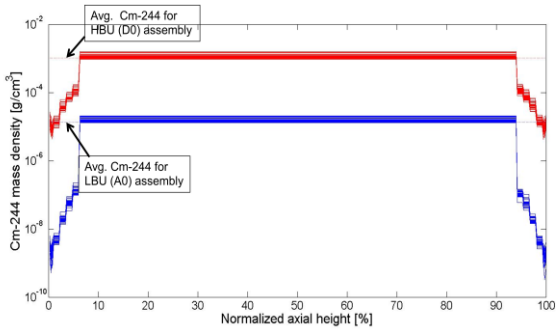

Fig. 4. ^{244}Cm mass densities as a function of the normalized axial height for the D0 (HBU, red) and the A0 (LBU, blue) assemblies

The ^{244}Cm mass density in the fuel rods of the same two assemblies is shown in Fig. 4. The general tendency of the ^{244}Cm mass density distribution is similar to that of the Pu mass density because the first isotope in the reaction chain that generates ^{244}Cm is ^{239}Pu, the dominant isotope of plutonium present in the spent fuel. The maximum ^{244}Cm mass density for the HBU is 1.60E-3 [g/cm^3], which is around 385 times greater than the minimum mass density, 4.16E-6 [g/cm^3]. In the LBU, the maximum value, 2.05E-5 [g/cm^3], is 6270 times greater than the minimum value, 3.27E-10 [g/cm^3]. Greater difference in the mass density between the maximum and minimum vales is observed for ^{244}Cm than Pu.

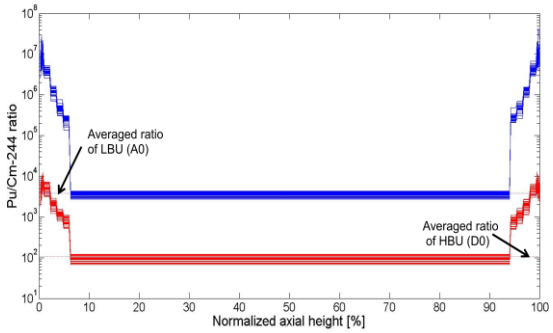

Fig. 5. The Pu-to-^{244}Cm ratios as a function of the normalized axial height for the D0 (HBU, red) and A0 (LBU, blue) assemblies.

In order to utilize Eq. (1) for the purpose of Pu mass measurement, we need to determine the Pu-to-^{244}Cm ratio. Fig. 5 illustrates the Pu-to-^{244}Cm ratio for individual fuel rods in two assemblies as a function of the normalized axial height, based on the results shown in Figs. 3 and 4. In general, the ratio for the LBU is greater than the HBU. The maximum and minimum ratios are 1.30E4 and 6.84E1 for the HBU. The ratio determined by the averaged Pu and ^{244}Cm mass densities in the HBU assembly is 1.06E2, which is 123 times smaller than the maximum value and 1.55 times greater than the minimum value. In the LBU, 4.44E7 and 2.76E3 are the maximum

and minimum ratios, respectively. The average ratio, 3.85E3, is 11500 times smaller than the maximum ratio and 1.39 times greater than the minimum ratio. Thus, significant difference in the ratios along the axial direction for two different burnup cases is observed.

IV. QUANTITATIVE MATERIAL ACCOUNTING

IV.1 Pyroprocess Stages Considered

The information and understanding about the non-uniformity of nuclide compositions in the spent fuel assembly as observed in the simulations described in the previous section, is to be utilized to evaluate material accountancy in the pyroprocessing. This can be done by first considering actual material processes that are included in the pyroprocessing system, including various separations and mixing processes. By these processes, material non-uniformity will be significantly altered. In this section, among processes to be included in the pyroprocess system, we consider only the three stages, prior to the main processes of the pyroprocess, electro-refining and electro-winning. The three stages we consider are chopping, voloxidation, and homogenization.

Chopping is the process in which fuel pins are disassembled and chopped to expose fuel pellets to the ambient environment. In the present study, we consider a fuel pellet with height of 1 cm as the smallest unit of materials, within which the nuclide composition is assumed homogeneous. In the Serpent simulation, the fuel rod is divided into 1 cm long meshes in axial direction at the top and bottom, corresponding to the size of a fuel pellet. The largest mesh (335 cm) is applied for the middle part of the fuel rod, allocating 335 pellets of the identical composition. There are 381 fuel pellets in one rod, and because there are 236 fuel rods in an assembly, the total number of pellet for one assembly is counted to be 89,916.

In the voloxidation process, the UO_2 fuel pellet is oxidized to U_3O_8 powder (Ref. 17). According to this reference, the voloxidation experiment at KAERI was conducted with 20 kgHM UO_2 pellet. U_3O_8 powder after voloxidation was confirmed to be homogeneous because of the mixing blade, the mesh layers and the vibration system involved in the voloxidation process. The mass, 20 kgHM UO_2, corresponds to around 10 fuel rods if the weight of one fuel rod is assumed 2 kg. Thus, 3810 pellets are handled in one batch.

We consider two cases for the material flow stream in the voloxidation process. In case 1, 10 fuel rods are randomly selected from an assembly and chopped. The chopped pieces from the 10 fuel rods go through the voloxidation process together. The nuclide composition of the powder would be equal to the averaged nuclide composition of 10 fuel rods, which are randomly selected. In case 2, all fuel rods in one assembly are chopped and 3810 fuel pellets are randomly selected to go through the voloxidation process.

After approximately 24 voloxidation batches, the output corresponding to a single assembly is mixed and homogenized in the homogenization process. After the homogenization process, the Pu and ^{244}Cm mass density of a sample powder should be equal to the averaged mass densities for the assemblies, shown in Figs. 3 and 4 as the horizontal dot lines, if the homogenization process is able to handle one assembly in one batch.

IV.2 Non-uniformity in the Pre-process Stages

Based on the above descriptions, the histograms for Pu and ^{244}Cm mass densities after each of the three pre-process stages of the pyroprocess system has been applied are plotted in Figs. 6 and 7. There are two figures, top (case 1) and bottom (case 2), with six different color bars. The histograms for the chopping and homogenization in the top and bottom figures are identical. Various colors are utilized to distinguish different combinations of the assembly types (HBU and LBU) and the pre-process stage. The vertical axis ranges between 0.0 and 1.0 for the normalized frequency. Pink and black lines exceed the range shown in the figures.

The histograms of the Pu mass density in the chopping process for HBU (red bar) and for LBU (blue bar) in Fig. 6 show broad distributions. The peaks correspond to the pellets included in the middle mesh of the fuel rods. The broad distribution is due to the contributions of the pellets located at the top and bottom of the fuel rods. The mean and standard deviation of the Pu mass density in the pellets for LBU and HBU assemblies are shown in Table 3.

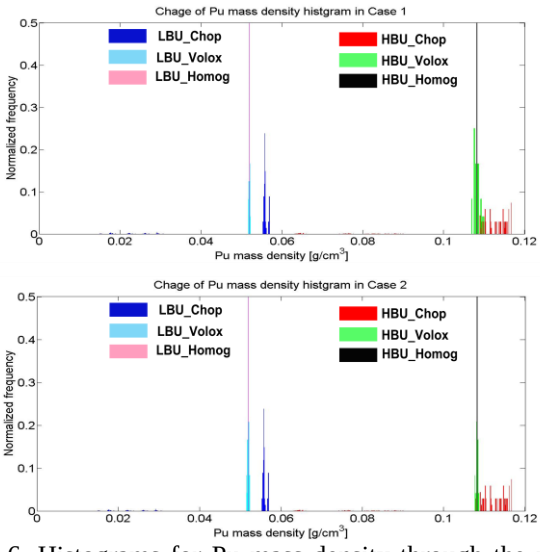

Fig. 6. Histograms for Pu mass density through the pre-process. Top: case 1; Bottom: case 2 of voloxidation.

The histograms for the ^{244}Cm mass densities are shown in Fig. 7. The peaks of the blue and red bars correspond to the pellets included in the middle mesh of the fuel rods. The broad distribution with low frequency is due to the contributions of the pellets located at the top and bottom of the fuel rods. The mean and standard deviation of ^{244}Cm in the pellets for LBU and HBU are shown in Table 4.

Table 3. Mean and standard deviation of the Pu mass density for each process in the pre-process.

Mass density [g/cm3]	Chopping		Voloxidation			Homo-geniz-ation.
	Mean	SD	Case	Mean	SD	
HBU	1.08E-1	1.35E-2	1	1.08E-1	7.86E-4	1.08E-1
			2	1.08E-1	2.56E-4	
LBU	5.19E-2	1.09E-2	1	5.19E-2	1.35E-4	5.19E-2
			2	5.19E-2	2.09E-4	

Table 4. Mean and standard deviation of the ^{244}Cm mass density for each process in the pre-process.

Mass density [g/cm3]	Chopping		Voloxidation			Homo-geniz-ation
	Mean	SD	Case	Mean	SD	
HBU	1.02E-3	3.97E-4	1	1.02E-3	5.33E-5	1.02E-3
			2	1.02E-3	7.59E-6	
LBU	1.35E-5	5.42E-6	1	1.35E-5	6.23E-7	1.35E-5
			2	1.35E-5	1.03E-7	

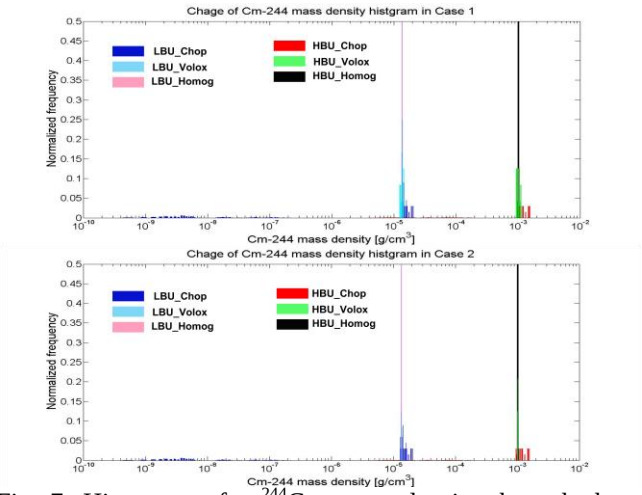

Fig. 7. Histograms for ^{244}Cm mass density through the pre-process. Top: case 1; Bottom: case 2 of voloxidation.

The histogram for the Pu-to-^{244}Cm ratio has been plotted for each process and each assembly as shown in Fig 8. The trend of histogram is similar to that of Pu and ^{244}Cm mass density. The peaks with the blue bar (LBU in chopping) and red bar (HBU in chopping) are due to the contribution of the pellets located in the middle mesh of the fuel rods. The low frequencies with the large variance are due to the contributions of the pellets included in the top and bottom of the fuel rods. The statistical summary for the ratio are shown in Table 5. The means of Pu-to-^{244}Cm ratio in chopping for LBU and HBU are different from that of homogenization. The mean ratio in the chopping stage is calculated by the average of each pellet's ratio in one assembly, as shown in Eq. (2), whereas the ratio after homogenization is calculated by the averaged Pu mass density of the assembly divided by the averaged ^{244}Cm mass density of the assembly, as shown in Eq. (3). In addition, the mean mass density in the voloxidation stage is calculated by the average mass density of 10 randomly selected fuel rods (case 1) or the average mass density of 3810 randomly selected pellets (case 2). The mean Pu and ^{244}Cm mass densities of the two cases in voloxidation are equal to those of the homogenization stage.

$$\text{Mean}\left[\frac{\text{Pu}}{^{244}\text{Cm}}\right]_{\text{Chop.}} = \frac{\left(\frac{\text{Pu}}{^{244}\text{Cm}}\right)_{p\_1} + \left(\frac{\text{Pu}}{^{244}\text{Cm}}\right)_{p\_2} + \left(\frac{\text{Pu}}{^{244}\text{Cm}}\right)_{p\_3} + \cdots + \left(\frac{\text{Pu}}{^{244}\text{Cm}}\right)_{p\_N}}{\text{N}} \quad (2)$$

where, N : Number of total pellets in one assembly
p_i : i-th pellet (i=1,2,…,N)

$$\text{Mean}\left[\frac{\text{Pu}}{^{244}\text{Cm}}\right]_{\text{Homog.}} = \frac{\text{Averaged Pu amount in the assembly}}{\text{Averaged } ^{244}\text{Cm amount in the assembly}} \quad (3)$$

Table 5 Mean and standard deviation of the Pu-to-^{244}Cm ratio for each process in the pre-process.

Pu-to-244Cm ratio	Chopping		Voloxidation			Homo-geniz-ation
	Mean	SD	Case	Mean	SD	
HBU	4.02E2	1.07E3	1	1.06E2	6.29E0	1.06E2
			2	1.06E2	5.90E-1	
LBU	2.97E5	1.42E6	1	3.85E3	1.71E2	3.85E3
			2	3.85E3	1.54E1	

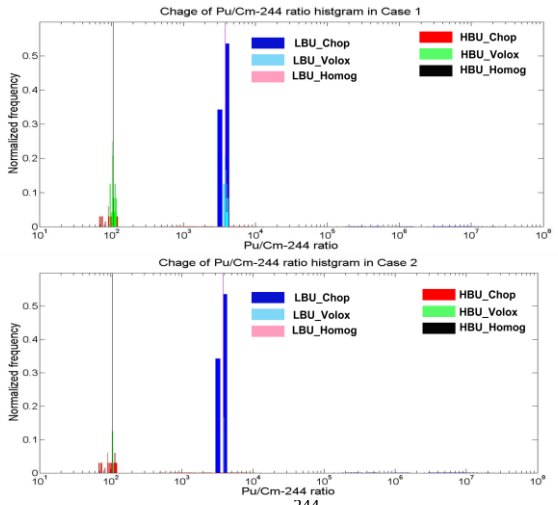

Fig. 8. Histogram for the Pu-to-^{244}Cm ratio through the pre-process. Top: case 1; Bottom: case 2 of voloxidation.

IV.3 Discussions

After chopping one assembly, there will be more than ten thousand cylindrical pieces, each measuring about a few centimeters in length. According to the result, the Pu-to-^{244}Cm ratio has significant difference among fuel assemblies as well as among fuel pins within the

same fuel assembly. Therefore the statistics of the distribution are substantially different before and after the chopping,. Depending on how the chopped pieces are picked up and a batch for voloxidation is formed, after the voloxidation the distribution of the ratio differs significantly. If we apply a wrong estimate for the ratio, the Pu mass in the batch can easily be over or underestimated by Eq. (1).

After chopping, smaller pieces could enhance the recovery rate of powder relative to larger pieces (Ref. 18), whereas more clandestine material stealing with the smaller pieces would be considerable. Therefore, the length of the pieces produced during chopping should be taken into account with respect to both material accounting and diversion as well as recovery of useful material.

The physical forms or phases of the spent fuel change during chopping and voloxidation. For instance, the long fuel rods become small pieces during chopping, and the small pieces are transformed to the powder in the voloxidation process. Apparent transformation of physical forms could be advantageous in detecting clandestine actions. However, because the physical form of feed material for the homogenization process is the same as that of the product, detection of such actions is more difficult in the homogenization stage than in the other stages.

As we have confirmed the importance of obtaining the mass density distribution as accurately as possible for the purpose of material accountancy, the numerical scheme for the depletion simulation should be reconsidered in that regard. In the present scheme, a large mesh is allocated at the center of the fuel pin, which has resulted in a sharp peak in the histograms for the mass density and the ratio. This is because the same value has been assigned to multiple pieces from the large center mesh. In reality, however, there should be non-uniform distribution within the large mesh. The depletion simulation should be done by dividing the large center mesh into multiple smaller meshes to more accurately reflect the real distribution.

V. CONCLUSIONS

The numerical recipe for the depletion simulation has been developed. The 15 meshes with different mesh sizes in the axial direction and a homogeneous mesh in the radial direction of the fuel rod have found to give accurate results for the subsequent study on material accountancy of the pyroprocess system.

Based on the developed recipes, the depletion simulations for two assemblies at extreme conditions of initial enrichment and the end-of-life burnup in the OPR-1000 reactor core have been conducted. Numerical results of the depletion simulation for the two assemblies indicate that significant non-uniformity of Pu and ^{244}Cm mass densities are observed in the axial direction, particularly, the top and bottom of the assemblies. The non-uniformity along the axial location is observed more significantly in the low burnup assembly than in the high burnup assembly. Future simulations should focus on dividing the large mesh at the center of each fuel to more accurately obtain the distribution.

The results from the depletion simulations for these two extreme cases have been utilized to observe how material non-uniformity changes after application of each of the pre-processes in the pyroprocess system. This was done by observing changes of the histograms for the mass densities of Pu and ^{244}Cm as well as that of the Pu-to-^{244}Cm ratio. Particularly for the voloxidation process, two cases have been considered and compared.

While the mean value of Pu and ^{244}Cm mass density of the pellets does not change from stage to stage, the standard deviation changes significantly, implying that the material accountancy could be significantly affected by how a batch is configured in the pre-process of pyroprocess. Conceptually, after the homogenization process, the Pu and ^{244}Cm mass densities become the same as the averaged mass densities of each assembly; however, it is not impossible to expect unequal values between the two due to measurement uncertainties or material unaccounted for (MUF).

The impact of uncertainty sources on the material accountancy will be discussed in the future.

ACKNOWLEDGMENTS

This works is supported and sponsored by Korea Atomic Energy Research Institute. The authors are grateful for discussions and suggestions from Mr. Milos Atz of UC Berkeley, which were helpful for improving clarity of the present paper.

REFERENCES

1. IAEA, IAEA Safeguards Glossary 2001 edition, International Nuclear Verification Series No.3 (2001)

2. Jae-Hyung Yoo, Chung-Seok Seo, Eung-Ho Kim and Han-Soo Lee, “A Conceptual Study of Pyroprocessing for Recovering Actinides from Spent Oxide Fuels”, *Nuclear Engineering and Technology*, Vol. 40, No. 7, p. 581-592 (2008).

3. N. Miura, H. O. Menlove, “The use of Cm neutrons to verify Pu in spent fuel and reprocessing wastes”, LA-12774-MS (1994).

4. P. C. Durst (PNNL), R. Wallace (LANL), I. Therios (ANL), M. H. Ehinger (ORNL), R. Bean (INL), D. N. Kovacic (ORNL), A. Dougan (LLNL), K. Tolk (SNL), B. D. Boyer (LANL), “Advanced Safeguards

Approaches for New Reprocessing Facilities", PNNL-16674 (2007).

5. Ryan N. Bratton, M. Avramova, and K. Ivanov, "OECD/NEA Benchmarking for Uncertainty Analysis in Modeling (UAM) for LWRs-Summary and Discussion of Neutronics cases (Phase I)", *Nuclear Engineering and Technology*, Vol. 46, No. 3, p. 313-342 (2014).
6. Liang Zhang, "Evaluation of High Power Density Annular Fuel Application in the Korea OPR-1000 Reactor", *Thesis of Master of Nuclear Engineering at MIT (2009*).
7. Yoshihira ANDO, Kenji NISHIHARA, and Hideki TAKANO, "Estimation of Spent Fuel Compositions from Light Water Reactors", *Journal of Nuclear Science and Technology*, Vol. 37, Issue 10 (2000).
8. J.C. Wagner and M.D. DeHart, "Review of Axial Burnup Distribution Consideration for Burnup Credit Calculations", *ORNL/TM-1999.246*, (2000).
9. Flavio Dante Giust, Peter Grimm, and Rakesh Chawla, "Experimental Validation of 3-D reconstructed Pin Power Distribution in Full-Scale BWR Fuel Assemblies with Partial-Length Rods", *Nuclear Science and Engineering*, 175, p.292-307 (2013).
10. Chan Bock Lee, Dae Ho Kim, Jae Seung Song, Je Gun Bang, and Youn Ho Jung, "RAPID Model to Predict Radial Burnup Distribution in LWR UO2 Fuel", *Journal of Nuclear Material*, 202, p. 196-204 (2000).
11. Jaakko Leppanen, "Serpent- a Continuous-energy Monte Carlo Reactor Physics Burnup Calculation Cdoe", User's manual (2013).
12. Seung Min Woo and Joonhong Ahn, "Model Development for Pu Mass Accountancy of Pyrometallurgical Processing with the Pu/Cm-244 ratio Method", *Actinide and Fission Product Partitioning and Transmutation 13th Information Exchange meeting(OECD/NEA)*, Seoul, Republic of Korea, September 23-26, 2014, OECD/NEA (2014).
13. M. D. DeHart, M. C. Brady and C. V. Parks, "OECD/NEA Burnup Credit Calculational Criticality Benchmark Phase I-B Results", ORNL-5621 (1996).
14. Wang, K., T-P Lou, E. Greenspan and J. Vujic, "Benchmarking and Validation of MOCUP", *Proc. of the International Topical Meeting on Advances in Reactor Physics and Mathematics and Computation into the Next Millennium, PHYSOR 2000*, Pittsburgh, Pennsylvania, May 7-11, 2000, American Nuclear Society (2000).
15. Seong-Kyu Ahn, Hee-Sung Shin, and Ho-Dong Kim, "Safeguardability Analysis for an Engineering Scale Pyroprocess Facility", *Journal of Nuclear Science and Technology*, Vol. 49, No.6, p. 632-639 June (2012).
16. Power Reactor Information System, IAEA, web site, http://www.iaea.org/PRIS/CountryStatistics/CountryDetails.aspx?current=KR (2014)
17. Young Hwan Kim, Hyo Jik Lee, Jong Kwang Lee, Jae Hoo Jung, Byung Suk Park, Ji Sup Yoon and Seong Won Park, "Engineering Design of a High-Capacity Vol-Oxidizer for Handling UO*2* Pellets of Tens of Kilogram", *Journal of NUCLEAR SCIENCE and TECHNOLOGY*, Vol. 45, No. 7, p. 617–624 (2008).
18. Young Hwan Kim, Ki-Ho Kim, Jar-Hoo Jung, Byung-Suk Park, Ji-Sup Yoon, and Hyo-Jik Lee, "Design of Remotely Operated Vol-oxidizer for Hot-cell Application", *Proceedings of 2009 IEEE International Symposium on Assembly and Manufacturing*, Suwon, Korea, 17-20 November (2009).